PROCEEDINGS OF SCIENCE

# On the performance of air shower reconstruction with the SKA-Low radio telescope

**A. Corstanje,**[d,e,*] **S. Bouma,**[b] **J.D. Bray,**[c] **S. Buitink,**[d,e] **V. De Henau,**[d] **M. Desmet,**[d] **E. Dickinson,**[f] **L. van Dongen,**[e] **T.A. Enßlin,**[g,h,i] **B. Hare,**[j,k] **H. He,**[l] **J.R. Hörandel,**[e] **T. Huege,**[a,d] **C.W. James,**[f] **M. Jetti,**[g,h] **P. Laub,**[b] **H.J. Mathes,**[a] **K. Mulrey,**[e,m] **A. Nelles,**[b,n] **S. Saha,**[a,o] **O. Scholten,**[j] **S. Sharma,**[b] **R.E. Spencer,**[c] **C. Sterpka,**[k] **S. ter Veen,**[k] **K. Terveer,**[b] **T.N.G. Trinh,**[q] **P. Turekova,**[j,k] **D. Veberic,**[a] **K. Watanabe,**[a] **M. Waterson,**[r] **C. Zhang,**[s,t] **P. Zhang**[u] **and Y. Zhang**[l,v]

*E-mail:* a.corstanje@astro.ru.nl

The Square Kilometre Array Observatory (SKAO) is a radio telescope currently under construction in South Africa and Australia. Its low-frequency part (50-350 MHz), located in Australia, features nearly 60,000 antennas in a core region of about 1 km diameter. With such an extreme antenna density, surpassing e.g. LOFAR by two orders of magnitude, this observatory is well equipped to make the most precise radio measurements of individual air showers. A decade of experience with LOFAR serves as a foundation for a next major step in reconstruction precision. We present a simulation of the reconstruction capabilities, using CoREAS-simulated showers, a realistic model of the antennas, and of the Galactic noise background. We apply the method used at LOFAR for reconstruction the depth of shower maximum $X_{\mathrm{max}}$, measuring the energy fluence of the radio pulse in each antenna and using an ensemble of simulated showers to fit to the data. We consider the use of beamforming within this method, combining groups of nearby antennas to boost the signal-to-noise ratio. The reconstruction precision that follows is about 6 to 8 g/cm2 over a primary energy range of $10^{16}$ to $10^{18}$ eV, with a minimal bias from the reconstruction process. This sets a baseline to what can be achieved, both in energy range extension downward as in reconstruction precision, from methods that haven proven robust in practice. Further significant progress is expected, as new methods are being developed that measure the longitudinal shower profile in more detail than just its $X_{\mathrm{max}}$. We also discuss expected event rates given reasonable technical limitations, relating this to suitable numbers for a mass composition analysis in narrow energy bins.

39th International Cosmic Ray Conference (ICRC2025)
15–24 July 2025
Geneva, Switzerland

ICRC 2025
The Astroparticle Physics Conference
Geneva July 15-24, 2025

*Speaker





PoS(ICRC2025)230

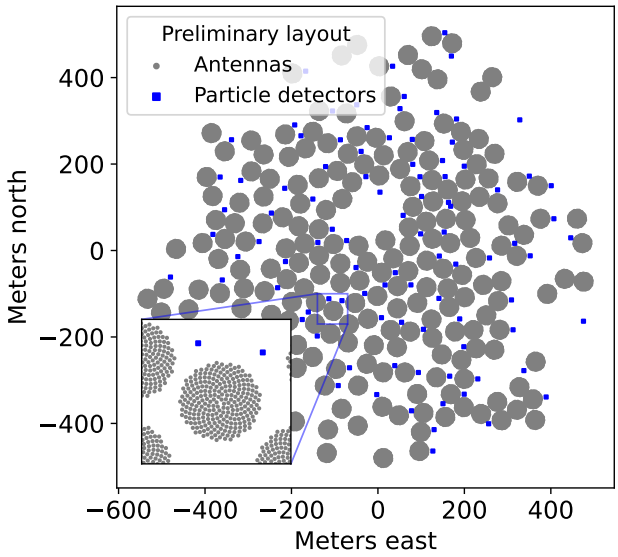


**Figure 1:** The inner core region of SKA-Low with the "AA*" antenna layout which is close to the full layout. 100 particle detectors of 1 $m^2$ (not to scale) have been positioned near antenna stations. Final positions are to be decided later based on on-site logistics.

## 1. Introduction

The Square Kilometre Array Observatory (SKAO) is currently being built in Australia (low frequencies) and South Africa (350 MHz to GHz frequencies). The layout of SKA-Low in Australia comprises about 57,000 wide-view antennas in an inner core of nearly 1 $km^2$, as shown in Fig. 1, operating in a 50 to 350 MHz frequency band. The plotted layout labeled "AA*" comprises about 90 % of the full array in the inner core region, and is set as a major milestone in its construction, to be reached 3 to 4 years from now.

An antenna density two orders of magnitude above LOFAR, which is already a dense array in terms of cosmic ray detection, presents a unique opportunity to measure air showers in the finest detail. In this analysis we explore its capabilities, by using established simulation and analysis techniques used at LOFAR, with minimal adaptations. Focusing on reconstructing the depth of shower maximum $X_{\mathrm{max}}$, this includes producing radio traces for all antennas, and adding background noise with a realistic power spectrum and absolute level. The process of measuring signal energy fluence per antenna, which is the basis for fitting an ensemble of simulations to data, is thus simulated realistically.

This sets a baseline for the performance of SKA-Low as a cosmic-ray detector; new analysis techniques that exploit information in the signals beyond the energy fluence are expected to improve on these results. The analysis is presented in more detail in [1].

## 2. Methods

Below we describe the simulation and reconstruction process, starting from CoREAS showers, applying antenna models and adding realistic background noise, measuring fluence, and recon-

structing $X_{\max}$.

### 2.1 Air shower simulations

We have produced an ensemble of 140 simulated showers with Corsika [2] and CoREAS [3] across 5 primary elements (50 H, 20 He, 20 C, 20 Si, 30 Fe). One ensemble was produced for each of 3 zenith angles 15, 30, and 40 degrees, arriving from East. These are used to perform the $X_{\max}$ reconstruction based on the method in [4] which also has been used extensively at LOFAR [5, 6].

Primary energy in the simulations was set to $10^{17}$ eV, and the radio traces were scaled in amplitude proportionally to a variety of primary energies. To evaluate the $X_{\max}$ reconstruction, we used each shower in turn as mock data, and reconstructed it using all other showers in the ensemble as model showers to fit to the data. The procedure was developed for LOFAR and is explained in more detail in [4]. The site parameters of SKA-Low were set, in particular altitude 378 m and magnetic field components $27.60\,\mu$T (horizontal) and $-48.27\,\mu$T (vertical). Radio traces were simulated on a radial grid ('star shape') comprising 208 antennas. As simulating nearly 60,000 antennas would be intractable, we make use of the full-trace interpolation method in [7] which was found to produce traces at a high accuracy suitable for SKAO work, and is available as open source [8].

### 2.2 From simulated electric fields to measured voltages

The simulations yield the electric field traces as they arrive at each antenna; to convert this to voltages as they are measured at the antennas, we apply the SKALA4 antenna model which describes the gain and phase characteristics of the SKA-Low antennas [9, 10]. To model the background noise in the voltage traces, we use the GSM2016 Galactic sky model [11] and the NuRadio software [10] that (incoherently) adds the contributions of the sources on the sky, passed through the antenna model. Instrumental noise is added as a flat-spectrum (thermal) contribution at 30 % of the Galactic noise power. Noise with this frequency spectrum and absolute level is added to each voltage trace, for a realistic treatment.

Having the voltage traces, we apply a de-dispersion filter that compensates for the phase characteristic of the antennas. This concentrates the pulse energy in time without changing its energy, which is suitable for time-domain based fluence measurements.

As the noise frequency spectrum is falling relatively steeply, as about $\nu^{-2.55}$, we also apply a noise whitening filter which compensates for this, making the noise spectrum flat and thus weighting the signal frequency spectrum by signal-to-noise ratio. We find that this helps in lowering the detection threshold in terms of the primary energy, and increases the accuracy of low-fluence measurements, thus avoiding bias in $X_{\max}$ reconstructions.

### 2.3 Fluence measurements and radio footprint

We measure the distribution of the pulse energy fluence on the ground, at the antennas, which forms a 'radio footprint' that is used to reconstruct $X_{\max}$ of a measured shower. Here, we define 'fluence' as the time integration of voltage-squared over the duration of the pulse. Hence, this concerns the energy in the measured signals, i.e. after the antenna response and the post-filters mentioned above.

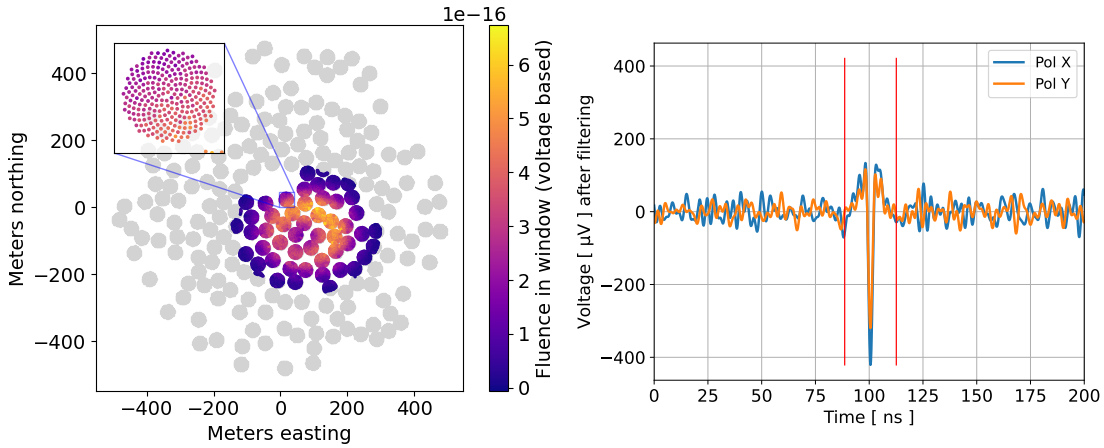


**Figure 2:** Left: A radio footprint from a $10^{17}$ eV proton, from voltage-based fluence measurements at individual antennas. Right: a time trace showing a short, symmetric pulse that is obtained after a de-dispersion filter has been applied. Vertical bars indicate the time window over which the energy is integrated.

In a noisy signal, we measure the fluence in a time window centered around the pulse maximum. Its length is taken as a compromise such that most of the fluence is captured, while keeping the amount of noise low. The average background level is subtracted, which for filtered Gaussian noise should give an unbiased fluence estimate. The uncertainty on the measured fluence is obtained from a Monte Carlo procedure, where we measure fluence 1000 times with different noise realizations, fitting the parameters of the functional form for uncorrelated Gaussian noise.

In Fig. 2, an example trace including noise, and an example radio footprint are shown.

### 2.4 Reconstruction of $X_{\mathrm{max}}$

The reconstruction of the depth of shower maximum is based on the fit method in [4], comparing the measured energy fluence per antenna in a chi-squared fit. We include antennas where the signal has an amplitude above $5\,\sigma$. The fit quality is defined as

$$\chi^2 = \sum_{\text{antennas}} \left( \frac{f_{\text{ant}} - A\, f_{\text{sim}}\,(x_{\text{ant}} - x_0,\, y_{\text{ant}} - y_0)}{\sigma_{\text{ant}}} \right)^2, \tag{1}$$

with measured fluence per antenna $f_{\text{ant}}$ and its uncertainty $\sigma_{\text{ant}}$, and fluence at the same positions in the model showers (passed through the antenna model, over the same time window) $f_{\text{sim}}$. The free parameters optimized in this fit are the core position $(x_0, y_0)$ and the overall scale factor $A$. This scale factor is needed for a proper $X_{\mathrm{max}}$ reconstruction, as without it, fit quality would be affected by differences in (electromagnetic) energy across model showers, irrespective of the footprint shape. Moreover, the fitted scale factor provides an estimate of the primary energy.

An example fit quality plot of an $X_{\mathrm{max}}$ reconstruction is shown in Fig. 3.

## 3. Results

We have evaluated the accuracy of the $X_{\mathrm{max}}$ reconstruction as a function of primary energy. The results are as depicted in Fig. 4. It shows that a precision level of 5 to 8 g/cm$^2$ is achieved

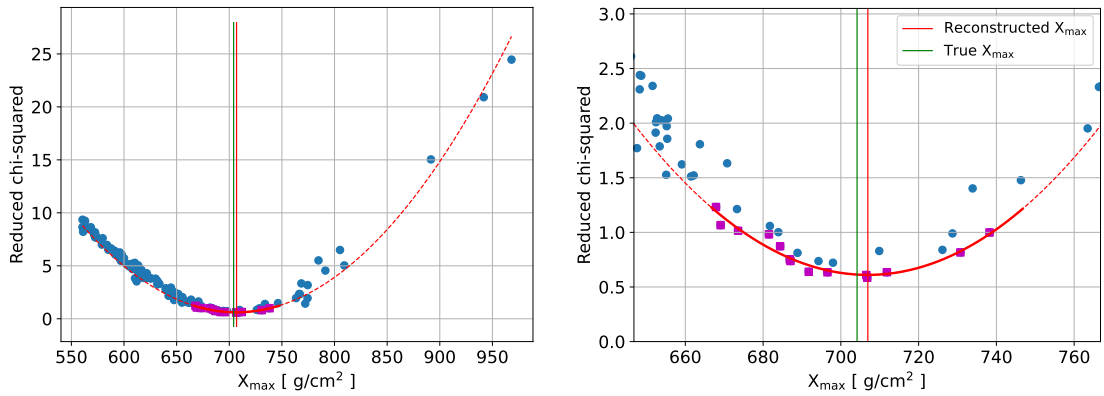


**Figure 3:** When plotting the fit $\chi^2$ versus $X_{\max}$, the points form a parabola around a minimum, to lowest order. Fitting this parabola from the lower envelope of the points gives the reconstructed $X_{\max}$.

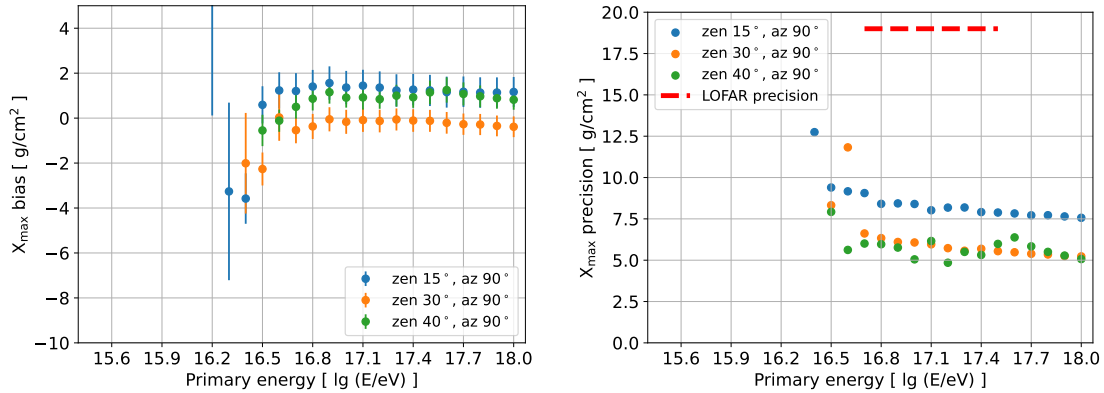


**Figure 4:** Bias (left) and precision (right) of the reconstructed $X_{\max}$, versus primary energy. One in four antennas of the array were used. The precision at LOFAR which is just below 20 g/cm$^2$ is shown for comparison.

down to a primary energy of $10^{16.5}$ eV. This can be compared to e.g. LOFAR, where precision is on average just below 20 g/cm$^2$. At lower energies, reconstructions start to fail due to too low signal-to-noise ratios (SNR).

Bias levels due to the reconstruction procedure are below 1.5 g/cm$^2$. Some ensemble-specific details may matter, such as a lower density of showers at high $X_{\max}$ (the values at each energy are from the same ensemble, scaled to mimic a given primary energy). We have removed the 5 lowest and 5 highest $X_{\max}$ values, so 10 out of 140 showers. At LOFAR [5, 6] we simulated extra showers pre-selected to have an $X_{\max}$ close to each $X_{\max}$ estimate, which helps to avoid such inaccuracies in a practical setting.

At high energies, the precision reaches a plateau; it is not limited by the number of antennas or by SNR, but by other shower parameters which are neglected when only focussing on $X_{\max}$. Further improvement is expected when reconstructing more parameters, see e.g. [12–15].

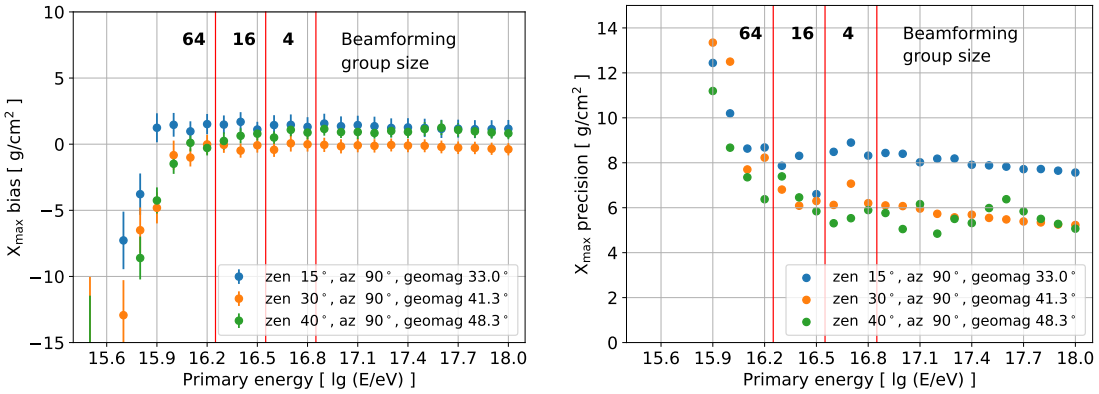


**Figure 5:** Same as Fig. 4, now with group-wise beamforming. The group sizes are indicated by the numbers within the red vertical lines.

### 3.1 Extending the energy range using group-wise beamforming

We have emulated the process of beamforming groups of 4, 16, and 64 neighboring antennas by decimating the number of antennas by this factor and increasing the amplitude SNR by its square root. As seen in Fig. 5, this pushes the low-energy reliable detection limit downward considerably, to at least $10^{16}$ eV while retaining accuracy. Beamforming methods that make use of all antennas relevant for a given shower will likely improve on this [16, 17].

## 4. Considerations for mass composition measurements at SKA-Low

We have investigated what the requirements are for a dataset from SKA-Low to make a mass composition estimate that would be a major improvement over the published LOFAR results [6]. Again, this would be using the same methods based only on $X_{\mathrm{max}}$. Two considerations are key: (1) to have uncertainties dominated by systematics, i.e. not being limited by low or moderate number statistics. And (2) to have a mass composition estimate in narrow energy bins, for instance at width 0.1 in $\log(E/\mathrm{eV})$, to see the trends with energy.

To this end we have done a parametric bootstrap analysis using the best-fit mass composition found at LOFAR, generating a set of $N$ $X_{\mathrm{max}}$ values with statistical errors in line with the precision results above. Assuming for now the same total level of systematic errors as at LOFAR, i.e. 9 g/cm$^2$, we have run the same mass composition analysis code to see the effect on the error bars. As seen in Fig. 6, for roughly $N = 1000$ the result is clearly systematics-limited, and increasing the sample size (even e.g. to $N = 10000$) does not improve the results significantly. Also, at $N = 1000$, uncertainties on average $X_{\mathrm{max}}$ and on the standard deviation of $X_{\mathrm{max}}$ are about 2 and 3 g/cm$^2$ respectively, which is satisfactory.

Turning from what is desired to what nature and the observatory can provide, we considered the cosmic-ray energy spectrum, which in our energy range is reasonably approximated by a power law with a spectral index $-3$. Taking the values from [18], we obtain the results in the right panel of Fig. 6. Here, the values are expressed in event counts per energy bin of width 0.1 in $\log(E/\mathrm{eV})$, per net observing year, for now neglecting possible bias and quality cuts. Numbers that enter into this

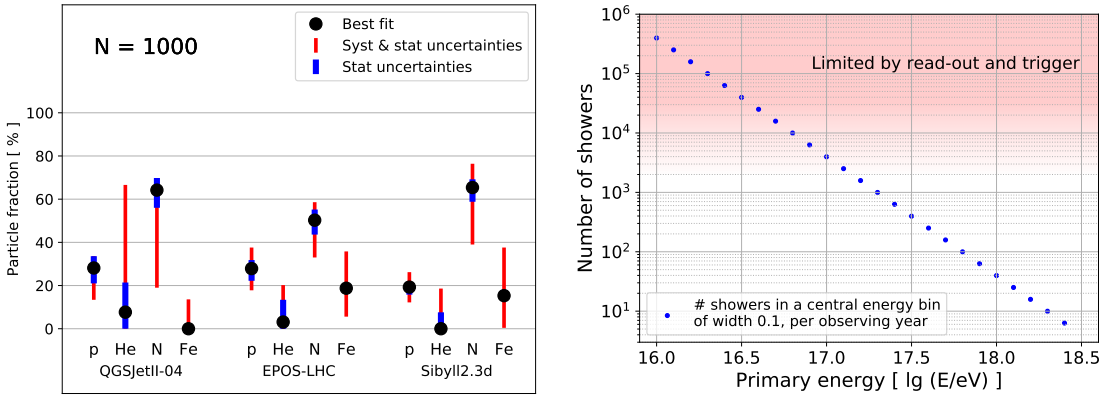


**Figure 6:** Left: an example mass composition estimate from a bootstrapped sample of $N = 1000$. At this sample size, the estimate is limited by systematic uncertainties, and a further increase in size has little effect. Right: an approximate cosmic ray spectrum expressed in number of events per energy bin per net observing year. It crossed $N = 1000$ around $\lg(E/eV) = 17.3$.

calculation are the area of the SKA-Low inner core and a zenith angle range from 0 to 55 degrees, which are about 0.8 km$^2$ and 2.7 sr respectively.

Hence, up to $10^{17.3}$ eV, the desired level of 1000 events is satisfied within one observing year. For higher energies, one naturally needs longer observing times and/or wider energy bins.

In terms of technical requirements, setting a cap to 1000 events per bin leads to an event count of roughly 15,000 events per observing year, which amount to triggering twice an hour. This is important to note, as running a cosmic-ray observing mode on an operational radio telescope facility is a continuous background process that must not interfere with ongoing astronomical observations. Triggering twice an hour, and subsequently downloading on the order of 1 GB of data from the buffers, should have only a marginal impact on the system which is designed for very large data throughputs.

## 5. Summary

We have made a first baseline estimate of the performance of SKA-Low as a cosmic ray radio detector. To this end, we have applied the methods developed to maturity for LOFAR, with minimal adaptations. Main results include a precision on $X_{\max}$ of 5 to 8 g/cm$^2$ above a primary energy of $10^{16.5}$ eV with negligible bias from the reconstruction. By using beamforming of groups of adjacent antennas, the reliable detection threshold is lowered to $10^{16}$ eV; with more sophisticated beamforming methods this is expected to be lowered even further.

Considering the requirements for obtaining an accurate mass composition analysis with fine-grained energy resolution, we find that up to about $10^{17.3}$ eV a suitable dataset can be collected in one year of net observing time. Technical limitations imposed by running a cosmic-ray detection mode alongside various astronomical observations are not expected to be reached when collecting such a dataset; trigger rates and data volumes are only marginal in the context of a data-intensive radio telescope. At low energies however, cosmic rays are quite abundant and a cap on triggering data readouts may be necessary there.

From the plateau in the precision results at higher energies, and from the systematics-limited mass composition results, we find that SKA-Low will reach the limits of the current analysis methods focusing only on $X_{\max}$. Studies into various more advanced methods are ongoing, and SKA-Low is an ideally suited instrument to make progress in this direction.

## References


[1] A. Corstanje *et al.* *Physical Review D* (June, 2025) .

[2] D. Heck, J. Knapp, J. N. Capdevielle, G. Schatz, and T. Thouw, "CORSIKA: A Monte Carlo code to simulate extensive air showers," tech. rep., 2, 1998.

[3] T. Huege, M. Ludwig, and C. W. James *AIP Conf. Proc.* **1535** no. 1, (2013) 128.

[4] **LOFAR** Collaboration, S. Buitink *et al.* *Phys. Rev. D* **90** no. 8, (2014) 082003.

[5] **LOFAR** Collaboration, S. Buitink *et al.* *Nature* **531** (2016) 70.

[6] **LOFAR** Collaboration, A. Corstanje *et al.* *Phys. Rev. D* **103** no. 10, (2021) 102006.

[7] A. Corstanje *et al.* *Journal of Instrumentation* **18** no. 9, (Sept., 2023) P09005.

[8] `https://github.com/nu-radio/cr-pulse-interpolator`.

[9] `https://github.com/nu-radio/NuRadioMC/tree/develop/NuRadioReco/detector`.

[10] C. Glaser *et al.* *Eur. Phys. J. C* **80** no. 2, (2020) 77.

[11] H. Zheng *et al.* *Mon. Not. Roy. Astron. Soc.* **464** no. 3, (2017) 3486–3497.

[12] S. Buitink *et al.* *PoS* **ICRC2023** (2023) 503.

[13] S. Buitink *et al.* *PoS* **ARENA2022** (2023) 046.

[14] A. Corstanje *et al.* *PoS* **ICRC2023** (2023) 500.

[15] A. Corstanje *et al.* *PoS* **ARENA2022** (2023) 024.

[16] H. Schoorlemmer and W. R. Carvalho *Eur. Phys. J. C* **81** no. 12, (2021) 1120.

[17] O. Scholten *et al.* *Phys. Rev. D* **110** no. 10, (2024) 103036.

[18] **Particle Data Group** Collaboration, S. Navas *et al.* *Phys. Rev. D* **110** no. 3, (2024) 030001.

## Affiliations

[a] Institut für Astroteilchenphysik, Karlsruhe Institute of Technology (KIT), P.O. Box 3640, 76021 Karlsruhe, Germany
[b] Erlangen Centre for Astroparticle Physics, Friedrich-Alexander-Universität Erlangen-Nürnberg, 91058 Erlangen, Germany
[c] Jodrell Bank Centre for Astrophysics, Department of Physics and Astronomy, University of Manchester, Manchester M13 9PL, UK
[d] Vrije Universiteit Brussel, Inter-University Institute For High Energies (IIHE), Pleinlaan 2, 1050 Brussels, Belgium
[e] Department of Astrophysics/IMAPP, Radboud University Nijmegen, P.O. Box 9010, 6500 GL Nijmegen, The Netherlands
[f] International Centre for Radio Astronomy Research, Curtin University, Bentley, 6102, WA, Australia
[g] Max-Planck Institut für Astrophysik, Karl-Schwarzschild-Str. 1, 85748 Garching, Germany
[h] Ludwig-Maximilians-Universität München (LMU), Geschwister-Scholl-Platz 1, 80539 München, Germany
[i] Deutsches Zentrum für Astrophysik, Postplatz 1, 02826 Görlitz, Germany
[j] Kapteyn Astronomical Institute, University of Groningen, P.O. Box 72, 9700 AB Groningen, Netherlands
[k] Netherlands Institute for Radio Astronomy (ASTRON), Dwingeloo, The Netherlands
[l] Key Laboratory of Dark Matter and Space Astronomy, Purple Mountain Observatory, Chinese Academy of Sciences, No. 10 Yuanhua Road, Nanjing, China
[m] Nikhef, Science Park Amsterdam, 1098 XG Amsterdam, The Netherlands
[n] Deutsches Elektronen-Synchrotron DESY, Platanenallee 6, 15738 Zeuthen, Germany
[o] Department of Physics, Indian Institute of Technology Kanpur, Kanpur, UP-208016, India
[p] Department of Physics, Khalifa University, P.O. Box 127788, Abu Dhabi, United Arab Emirates
[q] Physics Education Department, School of Education, Can Tho University, Campus II, 3/2 Street, Ninh Kieu District, Can Tho City, Viet Nam
[r] SKA Observatory, Jodrell Bank, Lower Withington, Macclesfield, SK11 9FT, UK
[s] School of Astronomy and Space Science, Nanjing University, Nanjing 210023, China
[t] Key Laboratory of Modern Astronomy and Astrophysics, Nanjing University, Ministry of Education, Nanjing 210023, China
[u] School of Electronic Engineering, Xidian University, No.2 South Taibai Road, Xi'an, China
[v] School of Astronomy and Space Science, University of Science and Technology of China, Hefei 230026, China

## Acknowledgements

SBo, AN and KT acknowledge funding through the Verbundforschung of the German Federal Ministry of Research, Technology and Space (BMFTR). PL, KW and MJ are supported by the Deutsche Forschungsgemeinschaft (DFG, German Research Foundation) – Projektnummer 531213488. MD is supported by the Flemish Foundation for Scientific Research (FWO-AL991). ST acknowledges funding from the Khalifa University RIG-S-2023-070 grant. SB acknowledges funding from the Medium-Scale Infrastructure program of the Flemish Foundation for Scientific Research (FWO). KM acknowledges funding from the Netherlands Research School for Astronomy (NOVA) Phase 6 Instrumentation Call. The authors gratefully acknowledge the computing time provided on the high-performance computer HoreKa by the National High-Performance Computing Center at KIT (NHR@KIT). This center is jointly supported by the Federal Ministry of Education and Research and the Ministry of Science, Research and the Arts of Baden-W¨urttemberg, as part of the National High-Performance Computing (NHR) joint funding program. HoreKa is partly funded by the German Research Foundation.